Available online on 15.12.2023 at http://jddtonline.info

Journal of Drug Delivery and Therapeutics

Open Access to Pharmaceutical and Medical Research

Open Access Full Text Article

Research Article

Exploration of 4-Chloro-3-nitrocoumarin: Spectroscopic Analysis, DFT Insights, Molecular Docking, Assessments of Antibacterial and *In Vitro* Anticancer Activities as a Potent Bioactive Agent

Surya S. Mohan[1], M.R. Meera[2,*], A. Rathika[3], R. Premkumar[4]

[1] *Research scholar (Reg.No.20213092132012), Department of Physics, Muslim Arts College, Thiruvithancode-629174, Affiliated to Manonmaniam Sundaranar University, Abishekapatti, Tirunelveli-627 012, Tamil Nadu, India.*

[2] *Associate Professor, Department of Physics, Sree Ayyappa College for Women, Chunkankadai, Nagercoil-629 003, Tamil Nadu, India.*

[3] *Department of Physics, Muslim Arts College, Thiruvithancode-629174, Tamil Nadu, India.*

[4] *Department of Physics, N.M.S.S.V.N. College, Madurai-625019, Tamil Nadu, India.*

Article Info:

Article History:

Received 04 Oct 2023
Reviewed 11 Nov 2023
Accepted 02 Dec 2023
Published 15 Dec 2023

Cite this article as:

Mohan SS, Meera MR, Rathika A, Premkumar R, Exploration of 4-Chloro-3-nitrocoumarin: Spectroscopic Analysis, DFT Insights, Molecular Docking, Assessments of Antibacterial and *In Vitro* Anticancer Activities as a Potent Bioactive Agent, Journal of Drug Delivery and Therapeutics. 2023; 13(12):189-200

DOI: http://dx.doi.org/10.22270/jddt.v13i12.6165

*Address for Correspondence:

Dr. M.R. Meera, Ph. D., Associate Professor, Department of Physics, Sree Ayyappa College for Women, Chunkankadai, Nagercoil 629 003, Tamil Nadu, India.

Abstract

The detailed theoretical and experimental (FT-IR, FT-Raman, UV-visible) spectroscopy analyses of the 4-Chloro-3-nitrocoumarin (CNC) molecule were carried out. The CNC compound's pharmacological properties were also investigated utilizing antibacterial and anticancer activity investigations. Initially, the CNC molecule was optimized by the density functional theory B3LYP method with a cc-pVTZ basis set using the Gaussian 09W program. The optimized molecular structure provides the harmonic vibrational frequencies of the CNC molecule. The observed and computed vibrational wavenumbers were assigned and found to be well correlated. UV-Vis absorption spectrum analysis indicates that the molecule contains π→π* electronic transition. Frontier molecular orbitals (FMOs) analysis indicates that the LUMO of CNC molecule is mainly located over the nitro group, it indicates that the nitro group is particularly prone to accepting electrons from other molecules and participate in chemical reactions where acts as an electrophile. Mulliken atomic charge distribution analysis further confirms the FMOs results. The antibacterial test results validate that the CNC molecule exhibits a stronger inhibitory effect on *Staphylococcus aureus* compared to the other tested bacteria. In vitro anticancer cytotoxicity analysis clearly evidences that the CNC compound inhibits the growth of HeLa cervical cancer cell lines more than A549 lung cancer cell lines. *In silico* molecular docking study further validates that the CNC molecule inhibits the function of the p38a Mitogen-activated protein kinase 14, which has been associated with cervical cancer. As a result, the present study paves the way for the development of new drugs to treat cervical cancer.

Keywords: 4-Chloro-3-nitrocoumarin; DFT; FT-IR; FT-Raman; Anticancer; Molecular docking; Cervical cancer drug.

1. INTRODUCTION

Cancer is a disease characterized by uncontrolled cell proliferation within the body. It is typically named after the specific area of the body where it initially develops, even if it later spreads to other regions. Significantly, the cervical cancer originates in the cervix, the connecting point between the vagina (birth canal) and the upper part of the uterus, where a developing fetus resides during pregnancy. While cervical cancer can affect anyone, it is more common among individuals over the age of 30. The primary cause of cervical cancer is often persistent infection with the human papillomavirus (HPV), a common virus transmitted through sexual activity. It's worth noting that at least half of those who are sexually active will encounter HPV at some point in their lives, but only a few women will develop cervical cancer.

To efficiently and cost-effectively comprehend the fundamental characteristics of biological molecules and medications, computational molecular modeling tools like density functional theory (DFT) calculations and molecular docking studies are invaluable. DFT simulations enable the study of a chemical system's reactivity, stable molecular geometry, vibrational frequencies, charge transfer stabilization interactions, and potential local reactive sites[1-3]. Local reactivity descriptors facilitate the understanding of how physiologically beneficial molecular systems interact, which, in turn, aids in the discovery of novel pharmacological substances and the development of more potent drugs[4,5].

Molecular docking, a computer-based method, allows for the evaluation of the compatibility between a ligand and a receptor-binding site. By predicting the binding mechanism and affinity of a ligand with proteins, molecular docking has become a pivotal tool in modern structure-based drug design. These considerations have led to the integration of DFT quantum chemical calculations and molecular docking studies for the molecule 4-Chloro-3-nitrocoumarin (CNC), a crucial component in subsequent *in vivo* research on this compound.

In recent years, well-diffusion antibacterial and *in vitro* anticancer investigations have gained prominence in the development of novel medications.

The Gaussian 09W software package and the B3LYP functional approaches were used in the current work to carry out the DFT quantum chemical computations. Experimental Fourier transform-infrared (FT-IR) and Fourier transform-Raman (FT-Raman) spectra of the CNC sample were compared with the computed infrared and Raman spectra of the CNC molecule. Additionally, a theoretical UV-Vis spectrum was generated and compared with experimental UV-Vis spectra. DFT computations were employed to analyze the Mulliken atomic charge distribution, frontier molecular orbitals (FMOs), Molecular electrostatic potential surface and Natural bond orbitals analysis of the CNC molecule[6,7].

2. MATERIALS AND METHODS

2.1 EXPERIMENTAL CHARACTERIZATIONS

The 99% pure CNC chemical was obtained from Sigma-Aldrich Chemicals Co. located in St. Louis, Missouri, United States. The Fourier transform-infrared (FT-IR) spectrum of the CNC compound was acquired using a KBr pellet technique at room temperature through a Perkin Elmer Spectrum 1 FT-IR spectrometer, featuring a resolution of 1.0 cm^{-1}. FT-Raman spectrum of the sample recorded using a BRUKER RFS 27 Stand-alone Raman spectrometer at room temperature and a resolution of 2 cm^{-1}. Both the FT-IR and FT-Raman spectra were recorded within the wavenumber range of 3500-400 cm^{-1}. For the UV-visible spectrum of the CNC compound, a Shimadzu UV-3600 ultraviolet (UV) visible Near Infrared spectrophotometer was utilized. This UV-Vis spectrum was recorded in the 200-600 nm range, with acetone serving as the solvent.

2.2 COMPUTATIONAL DETAILS

The molecular structure of the CNC molecule was optimized by DFT/B3LYP method with the cc-pVTZ basis set using the Gaussian 09W program[8]. Furthermore, the optimized molecular structure provided the vibrational wavenumbers for the CNC molecule. The VEDA 4.0 program was utilized to assign the calculated vibrational wavenumbers[9]. Subsequently, the time-dependent (TD)-DFT/B3LYP approach, in conjunction with the polarizable continuum model (PCM), was utilized to simulate the ultraviolet (UV) visible spectrum of the CNC molecule in an ethanol environment. The computed vibrational wavenumbers, UV-Vis spectra, Mulliken atomic charge distribution, and Frontier Molecular Orbitals (FMOs) were all visualized using the GaussView 05 visualization program[10]. It's worth noting that all computations were conducted at the ground state energy level of the CNC molecule, with no restrictions imposed on the potential energy surface except UV-Visible spectral simulation.

3. RESULTS AND DISCUSSION

3.1 MOLECULAR GEOMETRY AND SYMMETRY

The DFT/B3LYP methodology was initially employed for the optimization of the CNC molecular structure using the cc-pVTZ basis set. The global minimum energy for the CNC molecule was determined to be −1203.94 atomic units, and its optimized molecular structure is illustrated in Figure 1. Table 1 presents the computed values for bond lengths, bond angles, and dihedral angles in the CNC molecule. The CNC molecule exhibits C1 point group symmetry, confirming its non-centrosymmetric molecular structure. Figure 1 also reveals partial bond formations within the molecule, indicating electron transfer and an increase in its bioactivity. The CNC molecule exhibits distinct C-O bond lengths, with measurements of 1.39 Å for O1-C2, 1.35 Å for O1-C11, and 1.19 Å for C2-O9. The estimated C-C bond lengths for the CNC molecule, which closely correspond to the observed values, fall within the range of 1.37 Å to 1.48 Å. Notably, the shortest C-C bond is found between C3 and C4, while the longest C-C bond, which exceeds the other C-C bond lengths, exists between C2 and C3. The most electronegative oxygen atoms, O14 and O15 are attached with N13, and their bond lengths are 1.22 Å and 1.21 Å, respectively.

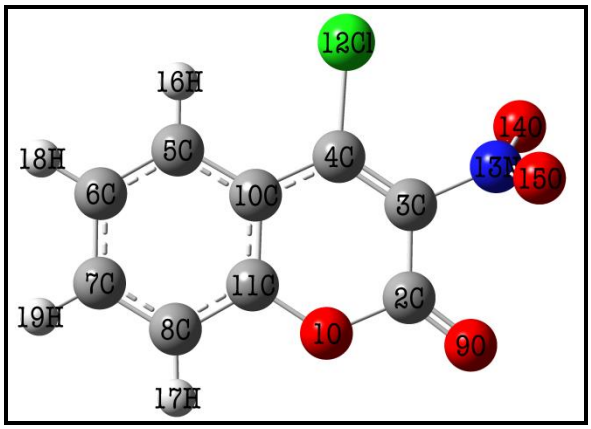

Figure 1: Optimized molecular structure of CNC molecule.

Table 1: Optimized structural parameters of the CNC molecule computed using DFT/B3LYP method with the cc-pVTZ basis set.

Structural Parameters	cc-pVTZ	Structural Parameters	cc-pVTZ	Structural Parameters	cc-pVTZ
Bond Length (Å)		**Bond Angle (Degree)**		**Dihedral Angle (Degree)**	
O1-C2	1.39	C10-C5-H16	119.19	C2-C3-N13-O15	-1.04
O1-C11	1.35	C5-C6-C7	120.13	C4-C3-N13-O14	-1.07
C2-C3	1.48	C5-C6-H18	119.79	C4-C3-N13-O15	178.96
C2-O9	1.19	C7-C6-H18	120.08	C3-C4-C10-C5	179.99
C3-C4	1.37	C6-C7-C8	120.44	C3-C4-C10-C11	0.01
C3-N13	1.49	C6-C7-H19	119.99	Cl12-C4-C10-C5	0.11
C4-C10	1.45	C8-C7-H19	119.57	Cl12-C4-C10-C11	-179.87
C4-Cl12	1.73	C7-C8-C11	119.16	C10-C5-C6-C7	0.01
C5-C6	1.38	C7-C8-H17	122.13	C10-C5-C6-H18	-180.00
C5-C10	1.41	C11-C8-H17	118.71	H16-C5-C6-C7	-179.99
C5-H16	1.08	C4-C10-C5	124.61	H16-C5-C6-H18	0.00
C6-C7	1.40	C4-C10-C11	117.48	C6-C5-C10-C4	-179.98
C6-H18	1.08	C5-C10-C11	117.90	C6-C5-C10-C11	0.00
C7-C8	1.38	O1-C11-C8	116.87	H16-C5-C10-C4	0.02
C7-H19	1.08	O1-C11-C10	121.51	H16-C5-C10-C11	180.00
C8-C11	1.39	C8-C11-C10	121.63	C5-C6-C7-C8	0.00
C8-H17	1.08	C3-N13-O14	117.83	C5-C6-C7-H19	180.00
C10-C11	1.40	C3-N13-O15	117.85	H18-C6-C7-C8	-180.00
N13-O14	1.22	O14-N13-O15	124.32	H18-C6-C7-H19	0.00
N13-O15	1.21	**Dihedral Angle (Degree)**		C6-C7-C8-C11	0.00
Bond Angle (Degree)		C11-O1-C2-C3	0.08	C6-C7-C8-H17	-180.00
C2-O1-C11	124.41	C11-O1-C2-O9	-179.89	H19-C7-C8-C11	180.00
O1-C2-C3	115.11	C2-O1-C11-C8	179.98	H19-C7-C8-H17	0.00
O1-C2-O9	116.20	C2-O1-C11-C10	-0.01	C7-C8-C11-O1	-179.98
C3-C2-O9	128.69	O1-C2-C3-C4	-0.1	C7-C8-C11-C10	0.01
C2-C3-C4	120.78	O1-C2-C3-N13	179.91	H17-C8-C11-O1	0.01
C2-C3-N13	116.12	O9-C2-C3-C4	179.87	H17-C8-C11-C10	-180.00
C4-C3-N13	123.10	O9-C2-C3-N13	-0.13	C4-C10-C11-O1	-0.03
C3-C4-C10	120.71	C2-C3-C4-C10	0.06	C4-C10-C11-C8	179.97
C3-C4-Cl12	124.39	C2-C3-C4-Cl12	179.92	C5-C10-C11-O1	179.99
C10-C4-Cl12	114.90	N13-C3-C4-C10	-179.95	C5-C10-C11-C8	0.00
C6-C5-C10	120.74	N13-C3-C4-Cl12	-0.08		
C6-C5-H16	120.08	C2-C3-N13-O14	178.92		

3.2 VIBRATIONAL SPECTRAL ANALYSIS

The optimized molecular structure of the CNC molecule comprises 19 atoms and exhibits 51 normal vibrational modes. The optimized molecular structure of the CNC molecule possesses C1 point group symmetry. Table 2 contains a list of the vibrational frequencies, IR intensity, Raman scattering activity, and matching vibrational assignments of the CNC molecule. To accommodate for the anharmonicity inherent in the DFT computations, scaling factors were employed to adjust the calculated vibrational frequencies[11].

The equation used for calculating the scaling factor of CNC employs 'C' as the scaling factor, where 'ν_i' and 'ω_i' represent the experimentally measured fundamental frequency and the corresponding theoretical harmonic frequency, respectively.

$$C = \Sigma(\nu_i * \omega_i)/\Sigma\omega_i^2$$

In the present case, scaling factors of 0.95 for stretching and 0.965 for bending vibrational modes were used, respectively. The observed and simulated infrared and Raman spectra of the CNC molecule were represented in Figs. 2 and 3, respectively. The deviation in the vibrational wavenumbers between the simulated and observed spectra is approximately 5%. Additionally, the enhanced stability of the CNC molecule is indicated by the absence of negative vibrational wavenumbers.

3.2.1 C-H VIBRATIONS

The C-H stretching vibrational modes of the phenyl ring are commonly identified in the range of 3100 to 3000 cm^{-1}. Notably, the phenyl ring C-H stretching vibrational mode exhibited medium peak at 3078 cm^{-1} in FT-Raman spectrum and calculated as 3078 cm^{-1} and a weak peak observed at 3050 cm^{-1} in FT-IR spectrum and the corresponding peak was calculated as 3055 cm^{-1}. The C-H in plane bending vibrational mode of the CNC molecule was observed as a medium peak at 1306 cm^{-1} in FT-IR spectrum and medium peak at 1325 cm^{-1} in FT-Raman spectrum. The corresponding peak was calculated as 1308 cm^{-1}[12].

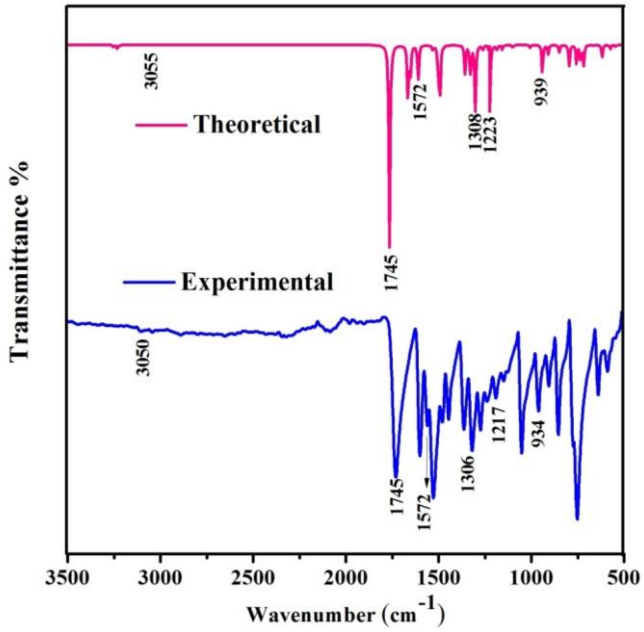

Figure 2: The infrared spectra of CNC molecule.

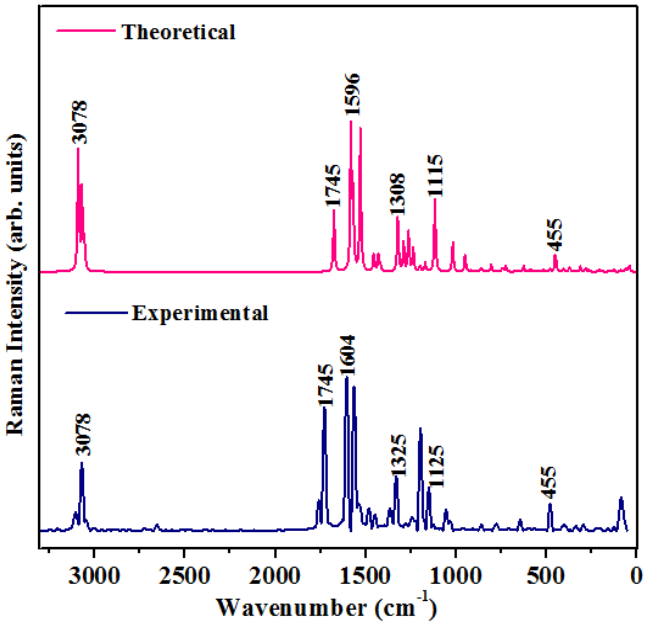

Figure 3: Raman spectra of CNC molecule.

Table 2: The calculated vibrational frequencies (cm^{-1}), IR intensities (Km mol^{-1}), Raman scattering activity ($Å^4$ amu^{-1}), reduced mass (amu), force constants (mDyne/$Å^{-1}$) and vibrational assignments based on PED calculations for the CNC molecule.

S. No	Observed Wavenumber cm^{-1})		Wavenumber (cm^{-1})		IR Intensity (Km mol^{-1})	Raman scattering activity ($Å^4$ amu^{-1})	Reduced Mass (amu)	Force Constant (mDyne/$Å^{-1}$)	Assignment with PED (%)
	FT-IR	FT-Raman	Calculated	Scaled					
1		3078s	3255	3078	4.25	225.39	1.1	6.85	ν ϕ CH (72)
2	3050w		3251	3055	1.1	30.36	1.09	6.81	ν ϕ CH (58)
3			3233	3039	8.74	162.63	1.09	6.73	ν ϕ CH (43)
4			3219	3025	2.77	65.34	1.09	6.64	ν ϕ CH (19)
5	1745vs	1745vs	1764	1745	468.94	84.87	12.89	23.65	ν C=O (68) + ν φ C=C (28)
6	1572s		1665	1572	131.08	217.43	6.25	10.2	ν C=O (10) + ν ϕ C=C (2)
7			1652	1552	61.13	96.72	9.96	16.01	ν C=O (32) + ν ϕ C=C (20)+ ν φ C=C (21)
9			1610	1513	77.77	189.69	5.77	8.81	ν ϕ C=C (18) + ν φ CC (19)
8			1531	1439	12.29	28.85	2.42	3.34	β ϕ CH (51)
10			1504	1413	31.23	21.71	2.38	3.17	β ϕ CH (68)
11			1494	1404	178.59	10.3	14.19	18.66	ν NO_2 (45)
12	1306m	1325m	1392	1308	0.76	77.75	10.27	11.72	β ϕ CH (94)

13			1358	1276	65.79	35.84	2.66	2.89	β ϕ CH(45)
14			1328	1248	76.66	59.56	2.37	2.46	β ϕ CH (32)
15	1217w		1302	1223	150.72	28.05	9.54	9.53	ν φ CN (52) + β ϕ CH (14)
16			1263	1187	14.05	8.83	3.2	3.01	ν ϕ CC (35) + ν ϕ CO (37) + β ϕ CH (21)
17			1231	1157	10.5	11	1.2	1.07	ν ϕ CC (44) + β ϕ CH (35)
18		1125m	1176	1125	3.38	87.64	4.92	4	β ϕ CH (44) + β ϕ C=C (19)
19			1168	1097	4.49	3.02	1.92	1.54	β ϕ CH (15) + β ϕ C=C (60)
20			1072	1007	6.78	35.84	2.15	1.46	ν ϕ CC (16) + β ϕ CH (15)
21			1038	975	0.09	0.05	1.34	0.85	η ϕ CH (24)

Table 2 (Continued)

S. No	Observed Wavenumber cm^{-1})		Wavenumber (cm^{-1})		IR Intensity (Km mol^{-1})	Raman scattering activity (Å^4 amu^{-1})	Reduced Mass (amu)	Force Constant (mDyne/Å^{-1})	Assignment with PED (%)
	FT-IR	FT-Raman	Calculated	Scaled					
22			1001	940	2.83	0.41	1.37	0.81	η ϕ CH (43)
23	934s		999	939	70.34	21.8	11.16	6.56	ν CCl (53) + ν φ CO (18)
24			966	908	20.71	1.55	8.33	4.58	ν CCl (42) + ν ϕ CO (11)
25			910	855	0.93	3.14	1.44	0.7	η ϕ CH (30)
26			903	848	16.57	2.37	9.61	4.62	ν ϕ CO (16) + β φ CCN (17)
27			847	796	48.61	7.67	8.98	3.8	ν φ CCl (56)+ β φ CCN (11)
28			805	756	41.93	0.35	1.6	0.61	η ϕ CH (46)
29			781	734	44.89	5.48	3.38	1.22	η ϕ CH (13) + τ ϕ CCCN (14)
30			763	717	46.6	5.46	10.71	3.68	ψ NO_2 (18)
31			757	711	1.38	1.13	5.24	1.77	η ϕ CH (34) + τ ϕ CCCC (13)
32			705	662	1.43	0.48	10.22	2.99	τ φ CCCN (18)
33			659	619	28.4	6.92	8.04	2.06	β ϕ CCC (30)
34			621	583	1.85	2.8	6.87	1.56	β ϕ CCC (27)
35			608	571	9.67	1.54	8.79	1.91	β φ CCl (40)
36			579	544	5.16	0.92	7.96	1.57	β ϕ CCC (32)
37			541	508	1.04	2.51	5.37	0.93	β ϕ CCC (24)
38			506	475	5.23	3.73	5.13	0.77	τ ϕ CCCC (30)
39		455w	473	455	3.36	26.15	10.09	1.33	τ ϕ CCCC (33)
40			425	399	1.53	3.68	4.39	0.47	τ ϕ CCCH (13) + τ ϕ CCCC (37)
41			390	366	3.31	5.2	10.39	0.93	ν ϕ CC (10) + β φ CCO (14)
42			328	308	1.62	5.79	11.9	0.75	β φ CCO (17) + β ϕ CCC (57)
43			296	278	0.2	3.69	11.53	0.6	β φ CCO (16) + β ϕ CCC (43)

Table 2 (Continued)

S. No	Observed Wavenumber cm^{-1})		Wavenumber (cm^{-1})		IR Intensity (Km mol^{-1})	Raman scattering activity (Å^4 amu^{-1})	Reduced Mass (amu)	Force Constant (mDyne/Å^{-1})	Assignment with PED (%)
	FT-IR	FT-Raman	Calculated	Scaled					
44			277	260	0.11	2.22	6.44	0.29	β φ CCO (22) + β ϕ CCC (43)
45			220	206	1.25	1.53	10.85	0.31	ν ϕ CC (16) + β ϕ CCC (29)

46			207	194	4.98	1.85	10.26	0.26	ν ϕ CC (46) + β ϕ CCC (39)
47			164	154	0.91	0.6	14.58	0.23	τ ϕ CCCC (11)
48			135	126	0.59	2.26	7.91	0.09	τ ϕ CCCC (41)
49			91	85	0.01	1.34	6.36	0.03	τ ϕ CCCC (35) + η ϕ CCCC (20)
50			61	57	0.05	3.88	11.44	0.03	τ ϕ CCCC (78)
51			42	39	0.16	5.71	14.86	0.02	β ϕ CCC (87)
w-weak, m-medium, s-strong, vs-very strong, ν - stretching; β - in-plane bending, η - out of plane bending, τ-torsion, ψ-scissoring, ϕ - benzene ring, φ - pyridine ring									

3.2.2 C=O VIBRATION

Characteristic vibrational modes for C=O stretching are found in the range of 1750 to 1650 cm^{-1}. The CNC molecule exhibited a very strong peak for the C=O stretching mode at 1745 cm^{-1} in both FT-IR and FT-Raman spectrum. The corresponding vibrational mode was calculated as 1745 cm^{-1}[13].

3.2.3 C-C VIBRATIONS

Vibrational modes for the C-C stretching within the phenyl ring are typically detected in the range of 1600 to 1430 cm^{-1}. A notable peak observed at 1572 cm^{-1} in the FT-IR spectrum is attributed to the molecule's C-C stretching vibrational mode of the CNC molecule and the corresponding peak was calculated as 1572 cm^{-1}. Moreover, the corresponding vibrational mode was calculated as 1552 and 1513 cm^{-1}[14].

3.2.4 C-CL VIBRATIONS

The usual C-Cl stretching vibrational modes fall within the range of 950 to 450 cm^{-1}. In the FT-IR spectrum of the CNC molecule, the C-Cl stretching mode was observed at 934 cm^{-1} and calculated as 939 cm^{-1}.

3.3 UV-VISIBLE ANALYSIS

In general, UV-visible spectrum analysis has the capability to forecast the electronic properties of organic compounds[15]. It provides insights into the characteristics of molecules in both their excited and ground states. In this case, the experimental UV-visible spectrum of the CNC molecule was recorded in liquid phase using ethanol solvent. Additionally, the UV-visible spectrum of the molecule was simulated using the TD-DFT method with the B3LYP/cc-pVTZ basis set. Fig. 4 depicts the observed and simulated UV-visible spectrum of the CNC molecule. Detailed information concerning the excitation wavelength (λ), excitation energy (E), oscillator strength (f), and corresponding orbital contribution for the CNC molecule is listed in Table 3. The findings reveal that the transition from the Highest Occupied Molecular Orbital (HOMO) to the Lowest Unoccupied Molecular Orbital (LUMO) is responsible for the most significant absorption peak of the CNC molecule, which was calculated at 324 nm, with an f-value of 0.0 and an E-value of 3.88 eV. It's noteworthy that experimentally, a similar peak was observed at 319 nm.

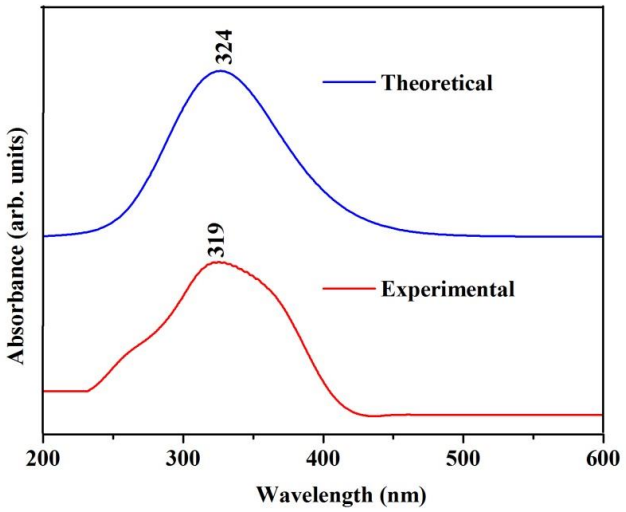

Figure 4: UV-Vis spectra of CNC molecule

Table 3: The calculated and observed UV-Vis spectral parameters in acetone solution for CNC molecule with its assignment

Calculated				Observed		Assignment
λ (nm)	E (eV)	F	Orbital contribution	λ (nm)	E (eV)	
324	3.88	0.0	H-6→L (22%), H-5→ L (41%), H-2→L (27%)	319	3.83	π→π*

3.4. MULLIKEN ATOMIC CHARGE DISTRIBUTION ANALYSIS

The Mulliken atomic charge distribution of a molecule greatly affects dipole moment and polarizability[16]. In this study, the DFT/B3LYP method with the cc-pVTZ basis set was used to simulate the Mulliken atomic charge distribution of the CNC molecule. Fig. 5 showed the Mulliken atomic charge distribution of the CNC molecule. The carbon atom C2 has high positive charge value (0.567) which is due to the C2 atom bonded with the electronegative oxygen atoms O1 and O9. The oxygen atom O1 (−0.559) of the CNC molecule has a high negative charge value. Moreover, the electronegative oxygen atoms in the CNC molecule have negative charge values except chlorine atom Cl12 and nitrogen atom N13 while all the hydrogen atoms in the molecule have positive charge values. The carbon atoms have both positive and negative charge values, which confirm the reactive nature of the molecule. However, the hydrogen atom H16 (0.178) and H17 (0.177) has a high charge value, suggesting that the H16 and H17 atoms contributes electrons to the carbon atom C5 and C8, respectively. Significantly, the electronegative chlorine atom Cl12 (0.234) has positive charge value which is due to the electron delocalization from the chlorine atom to the pyridine ring where the carbon atom C4 of pyridine ring becomes negative charge value (−0.258). As a result, the delocalization of charges within the molecule indicates the bioactive nature of the CNC molecule.

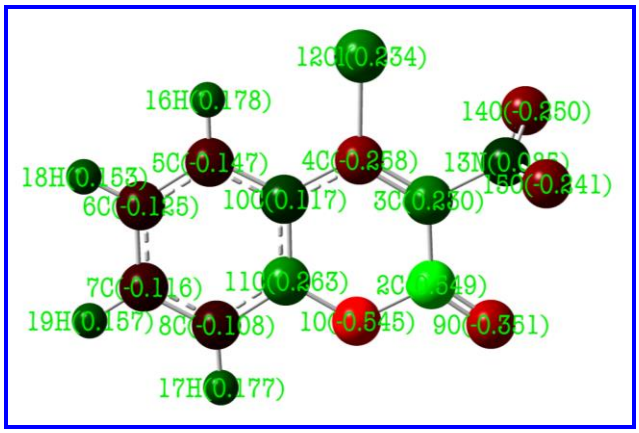

Figure 5: Mulliken charge distribution of CNC molecule

Table 4: Mulliken atomic charge values of CNC molecule

Atom	Mulliken Atomic charge	Atom	Mulliken Atomic charge
O1	−0.559	C11	0.263
C2	0.549	Cl12	0.234
C3	0.230	N13	0.095
C4	−0.258	O14	−0.250
C5	−0.147	O15	−0.241
C6	−0.125	H16	0.178
C7	−0.116	H17	0.177
C8	−0.108	H18	0.153
O9	−0.351	H19	0.157
C10	0.117		

3.5. FRONTIER MOLECULAR ORBITALS ANALYSIS

Frontier molecular orbitals (FMOs) are a commonly employed analysis used to describe a molecule's reactivity and its interactions with other molecules[17]. Typically, Koopmans' theorem is employed in FMO analysis to determine the chemical potential, hardness, electrophilicity, and electronegativity of organic compounds[13]. A molecule with a narrow energy gap is more reactive and susceptible to polarization. Fig.6 illustrates the simulated FMOs of the CNC molecule, where the positive and negative phases are represented by the colors red and green, respectively. Table 5 lists the insights into the HOMO and LUMO energies, the energy gap, and other FMOs related chemical characteristics of the CNC molecule.

The energy gap value of the CNC molecule is determined to be 3.83 eV, which confirms structural stability of the molecule. This information supports the analyses of molecular geometry and vibrational spectra. Furthermore, the calculated band gap energy value of the CNC molecule correlated with the reported bioactive molecules. Additionally, the CNC molecule's high ionization energy value (−7.28 eV) suggests its nucleophilic attack nature. The molecule's stability is indicated by the computed higher hardness value (1.92 eV) and lower softness value (0.52 eV). Thus, the CNC molecule's calculated electrophilicity index value (7.51 eV) indicates its improved electrophilic nature, which results the bioactive nature of the CNC molecule.

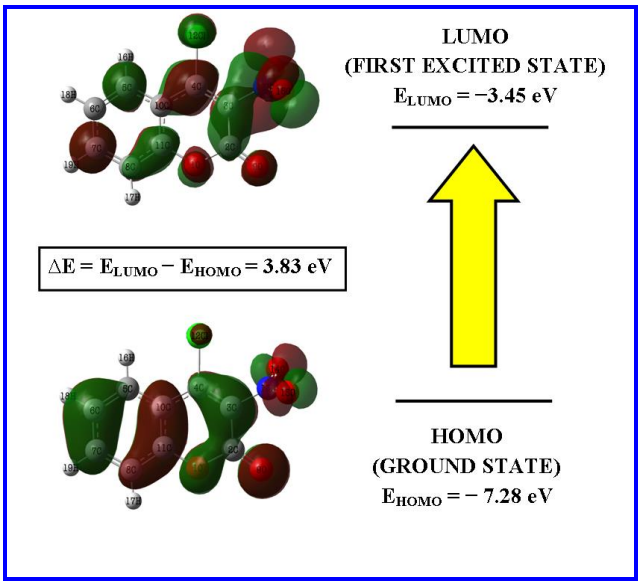

Figure 6: FMOs of CNC molecule

Table 5: The calculated FMOs related molecular properties of the CNC molecule

Molecular properties	Energy (eV)
E_{HOMO}	− 7.28
E_{LUMO}	− 3.45
Energy gap	3.83
Ionization energy (I)	7.28
Electron Affinity (A)	3.45
Global hardness (η)	1.92
Global Softness (S)	0.52
Chemical potential (μ)	−5.37
Electrophilicity index (ω)	7.51

3.6 NATURAL BOND ORBITAL ANALYSIS

Natural Bond Orbitals (NBO) analysis can provide valuable insights into hydrogen bonding and intra- as well as intermolecular charge transfer interactions of the molecules[18]. In this study, NBO analysis was performed using the DFT/B3LYP approach with the cc-pVTZ basis set, utilizing the NBO 3.1 program[19] integrated into the Gaussian 09 software. The stabilization energy E(2) associated with the delocalization of each donor (i) to an acceptor (j) within the CNC molecule was determined using second-order Fock matrix perturbation theory. These values are tabulated in Table S1. The stabilization interaction energy of the orbitals plays a crucial role in explaining intramolecular charge transfer and the formation of hydrogen bonds in the molecule. It is directly related to the energy difference between the interacting orbitals of effective donors and acceptors. Table S1 reveals that the CNC molecule's higher stabilization energy primarily arises from transitions involving the lone pair (LP) of O14 to π*(N13-O15), LP of O1 to π*(C2-O9), and π(C7-C8) to π*(C10-C11). In general, the common molecular characteristic of bioactive molecules is the stabilization interactions between LP orbitals and anti-bonding orbitals[20]. Consequently, the findings suggest that intramolecular charge transfer within the CNC molecule is mainly arises from LP to anti-bonding orbitals which confirm its reactivity and bioactivity.

3.7 MOLECULAR ELECTROSTATIC POTENTIAL (MEP) SURFACE ANALYSIS

A visual representation of a molecule's chemically active sites is provided by the total electron density mapped with MEP surface analysis, which also improves understanding of molecular reactivity, electrophilic reactions, substituent effects, and intra- and intermolecular interactions[21]. The MEP surface of the CNC molecule is depicted on Fig. 7. The MEP surface's red, yellow, light blue, and blue colours, respectively, designate the sections that are electron-rich, slightly electron-rich, slightly electron-deficient, and electron-deficient. Due to the oxygen atom's lone pair, it was discovered that the area surrounding the oxygen atoms was electron-rich (red). The hydrogen atoms H16, H17, H18, and H19 of the molecule, as well as H16, H17, and H19 were found in the electron-deficient (blue) area of the molecule. As a result of the MEP analysis, the hydrogen atom H19 in the benzene ring acts as potential electrophilic attack site, while the oxygen atom O9 in the pyridine ring is identified as potential nucleophilic attack site.

3.8 ANTIBACTERIAL ANALYSIS

The antibacterial activity of the CNC compound was assessed using the well diffusion method. In this experimental approach, the CNC compound was tested against four bacterial strains, namely, *Staphylococcus aureus, Klebsiella pneumoniae, Escherichia coli, and Pseudomonas aeruginosa*[22]. Fig. 8 illustrates the diameters of inhibitory zones for the CNC compound against these four bacterial strains, and the corresponding results are presented in Table 6. The antibacterial test results validate that the CNC molecule exhibits a stronger inhibitory effect on *Staphylococcus aureus* compared to the other tested bacteria

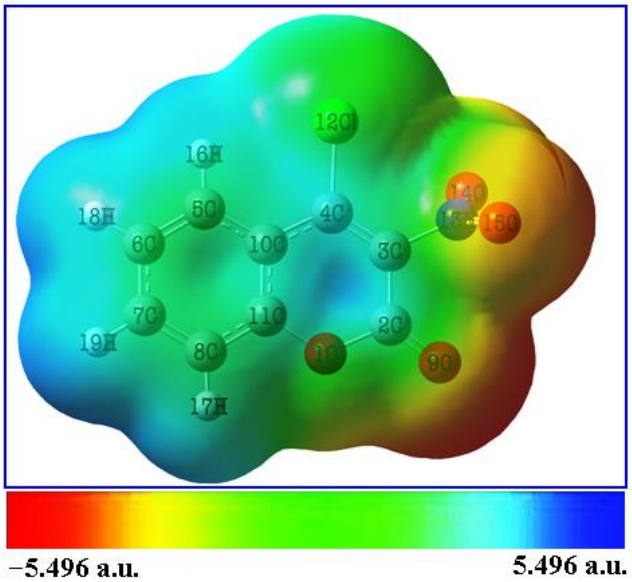

Figure 7: MEP surface of the CNC molecule

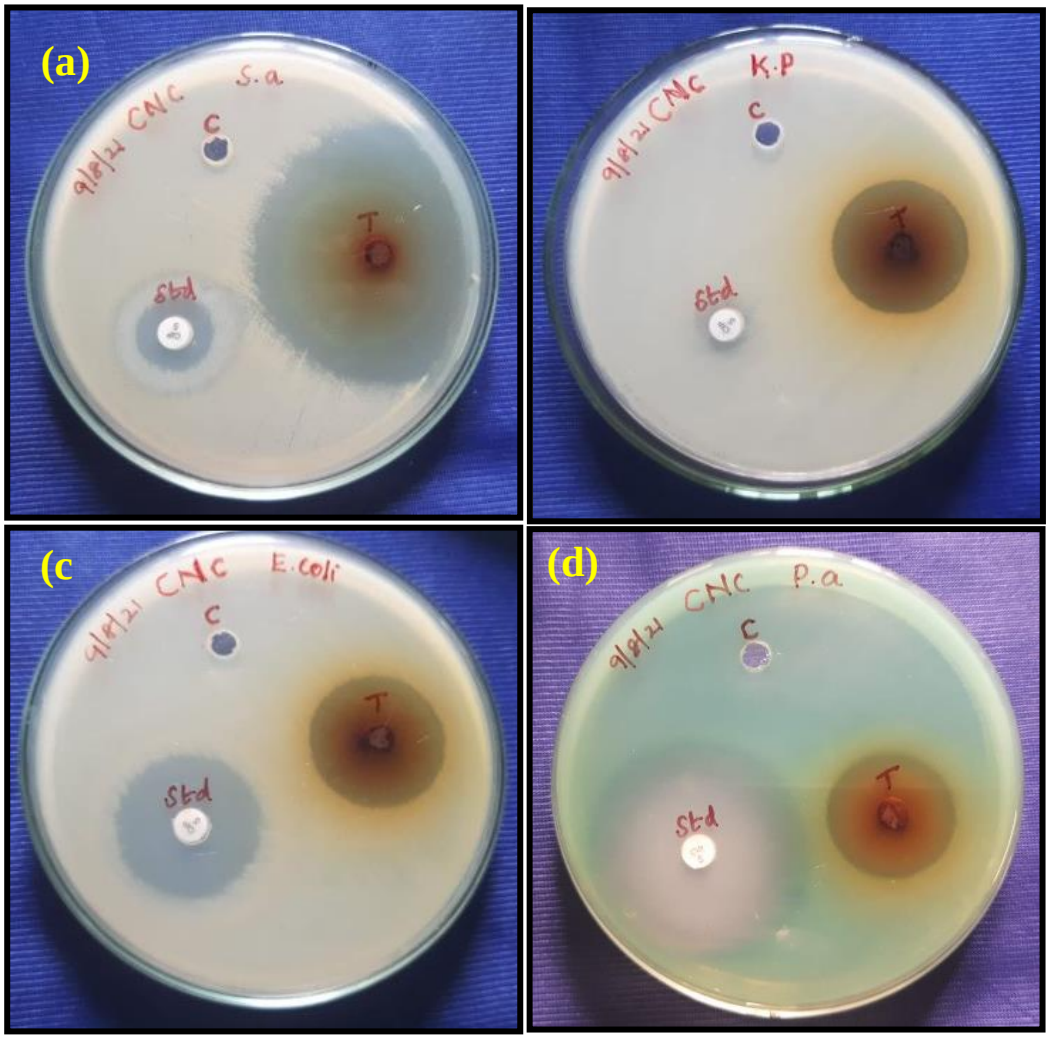

Figure 8: Diameters of inhibitory zones for the CNC compound against the four bacterial strains *(a) Staphylococcus aureus,* (b) *Klebsiella pneumonia, (c) Escherichia coli* and *(d) Pseudomonas aeruginosa*

Table 6: Diameters of inhibitory zones (mm) for CNC compound against four bacterial strains

Bacterial Strains	Zone of Inhibition (mm)		
	Control	Standard	Test
Staphylococcus aureus	NIL	15	50
Klebsiella pneumonia	NIL	9	29
Escherichia coli	NIL	23	27
Pseudomonas aeruginosa	NIL	29	25

3.9 IN VITRO CYTOTOXICITY ASSAY FOR ANTICANCER ACTIVITY

3.9.1 MTT ASSAY

The MTT assay analysis was used to analyze the cytotoxicity effect of HeLa (cervical) and A549 (lung) cancer cell lines after exposure to the CNC compound at concentrations ranging from 0-360 µg/ml for 24 hours[23,24]. The cell viability of HeLa and A549 cancer cell lines after incubation with CNC at various concentrations were shown in Figs. 9 and 10, respectively. After 24 hours of treatment with CNC at a concentration of 225 µg/ml, the cell viability of HeLa cells is about 40%. After 24 hours, the A549 cell viability is about 10% at a concentration of 225 µg/ml of CNC.

Interestingly, the IC_{50} value of the CNC compound were determined to be 3.34 µg/ml for the HeLa cancer cell line and 13.01 µg/ml for the A549 cancer cell line. These values indicate that the CNC compound exhibits a more potent inhibitory effect on the proliferation of HeLa cervical cancer cell lines compared to A549 lung cancer cell lines. Fig. 11 depicts the control and treated HeLa and A549 cancer cell lines with the CNC compound. Both treated cell lines display noticeable morphological changes, including cell swelling and rupture, as illustrated in Fig. 11. These observations suggest that the CNC compound may hold promise as an effective treatment for cervical cancer.

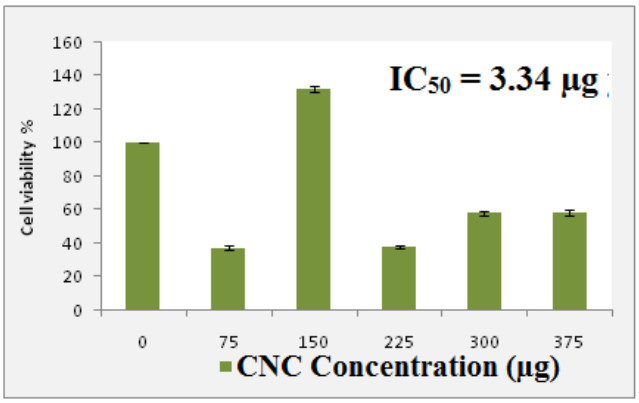

Figure 9: MTT assay measurement on different % of cell viability in HeLa cancer cell lines against varied concentrations of CNC compound.

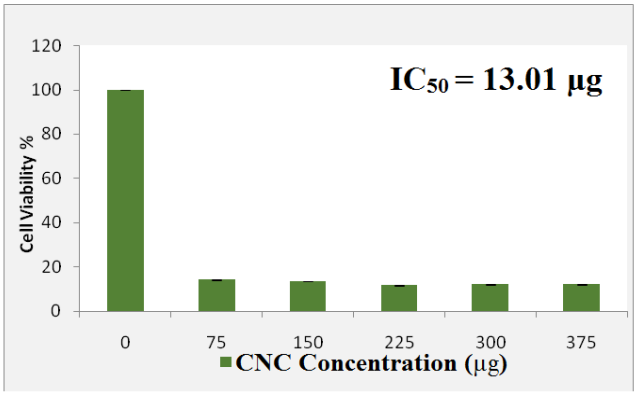

Figure 10: MTT assay measurement on different % of cell viability in A549 cancer cell lines against varied concentrations of CNC compound.

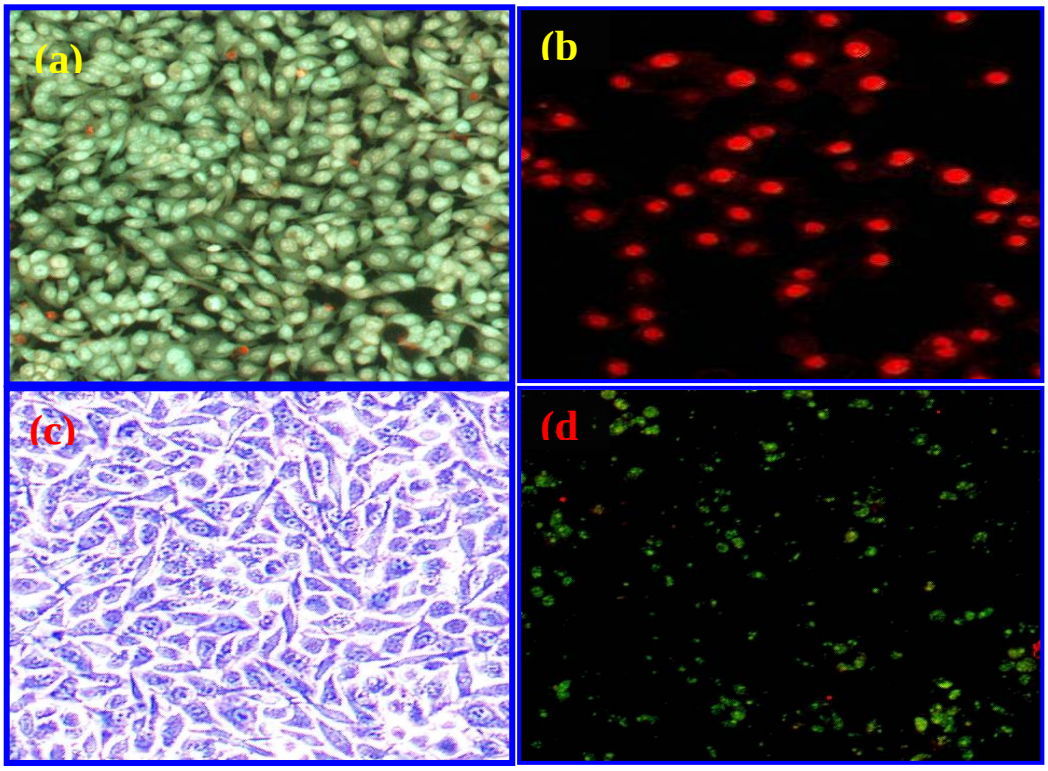

Figure 11: Morphological profile of the HeLa cells (a) control and (b) after treated with CNC compound for 24 hours and morphological profile of the A549 cells (a) control and (b) after treated with CNC compound for 24 hours.

3.10 MOLECULAR DOCKING ANALYSIS

Molecular docking is an effective method used to develop new drugs by using the structure-activity relationship (SAR) of a molecule[25]. Molecular docking analysis can predict important molecular docking characteristics such as binding energy, inhibition constant, and intermolecular energy of a ligand docked with a target protein. In general, different molecular docking approaches are accessible. The flexible ligand and rigid targeted protein docking analysis was done in this work. Furthermore, the title molecule (CNC) was employed as a ligand, human cervical cancer protein p38a Mitogen-activated protein kinase 14 (p38a MAPK) [PDB ID: 3FMK] and the human lung cancer proteins epidermal growth factor receptor (EGFR) [PDB ID: 2ITO] were used as targeted proteins. The ligand molecule was docked successfully with the targeted proteins. The lowest docked energy poses of the ligand (CNC) molecule with the respective targeted proteins were depicted in Fig. 12.

As depicted in Fig.12, the dotted yellow lines confirm the formation of hydrogen bonds between the ligand (CNC) and targeted proteins. In addition, hydrogen bond lengths and the amino acid residues in the targeted proteins were also depicted in Fig.12. Furthermore, the computed docking characteristics of the ligand with the targeted proteins, such as binding energy, inhibition constant and intermolecular energy, were given in Table 7 for the first three ranks (1, 2 and 3). These findings clearly suggest that the CNC molecule has a lower binding energy and inhibition constant values for the targeted protein, human cervical cancer protein p38a Mitogen-activated protein kinase 14 (p38a MAPK) [PDB ID: 3FMK]. These findings reveal that the CNC molecule can serve as an effective inhibitor of p38a Mitogen-activated protein kinase 14. Further, the molecular docking results support the experimental *in vitro* anticancer findings.

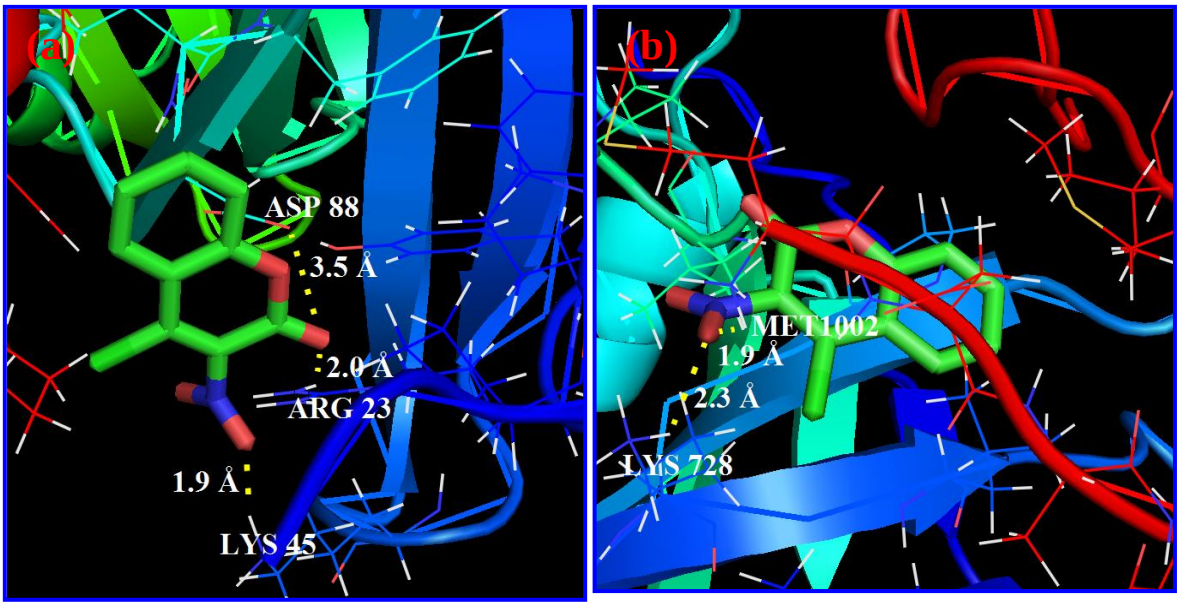

Figure12: The 3D representation of docked ligand (CNC) at the binding site of the targeted proteins (a) p38a MAPK and (b) EGFR.

Table 7: The obtained docking parameters of the CNC molecule on their rank were calculated by Autodock.

Ligand	Target protein (receptor)	Docking Parameters based on the rank								
		Binding energy (Kcal/mol)			Inhibition constant (μM)			Intermolecular energy (Kcal/mol)		
		1	2	3	1	2	3	1	2	3
CNC molecule	3FMK	−6.50	−5.90	−5.54	17.23	47.24	86.55	−6.80	−6.20	−5.84
	2ITO	−5.48	−4.74	−4.62	96.13	334.31	411.14	−5.78	−5.04	−4.92

4. CONCLUSION

The geometrical analysis of the CNC molecule was performed clearly. The precise vibrational assignments were carried out for the CNC molecule. The UV-Visible spectral analysis of the CNC molecule shows that there is an electronic transition between the benzene rings to chlorobenzene rings. This is a good sign for pharmacological applications. FMOs analysis further validated the bioactivity of the molecule by the evidence of charge transfer from the benzene rings to chlorobenzene rings. The MEP surface, Mulliken atomic charge distribution, and NBO investigations also supported the charge transfer from the benzene rings to chlorobenzene rings, demonstrating the bioactivity of the CNC molecule. The antibacterial analysis was performed and the obtained results confirm the CNC molecule exhibits a stronger inhibitory effect on *Staphylococcus aureus* compared to the other tested bacteria. In vitro anticancer cytotoxicity analysis was also performed and the results show that the CNC compound inhibits the growth of HeLa cervical cancer cell lines more than A549 lung cancer cell lines. *In silico* molecular docking study further confirm that the CNC molecule inhibits the function of the p38a Mitogen-activated protein kinase 14, which is associated with the cervical cancer. Thus, the present study paves the way for the development of new drugs to treatment of cervical cancer.

Table S1: Second order perturbation theory analysis of Fock matrix of CNC molecule by natural bond orbital analysis.

Donor (i)	ED (i) e	Acceptor (j)	ED (j) e	E(2)[a] (Kcal/mol)	E(j)-E(i)[b] (a.u)	F(i,j)[c] (a.u)
σ(C2-C3)	1.96757	σ*(C3-C4)	0.02751	5.18	1.31	0.074
σ(C2-C3)	1.96757	σ*(C4-Cl12)	0.03768	5.13	0.79	0.057
π(C2-O9)	1.97907	π*(C3-C4)	0.26502	6.54	0.36	0.046
π(C3-C4)	1.82997	π*(C2-O9)	0.29388	21.56	0.30	0.075
π(C3-C4)	1.82997	π*(C10-C11)	0.45451	9.45	0.32	0.053
π(C3-C4)	1.82997	π*(N13-O15)	0.59980	5.75	0.20	0.034
σ(C4-C10)	1.97280	σ*(C3-N13)	0.09592	4.87	0.99	0.063
π(C5-C6)	1.68516	π*(C7-C8)	0.29306	20.93	0.28	0.069
π(C5-C6)	1.68516	π*(C10-C11)	0.45451	18.68	0.25	0.064
π(C7-C8)	1.66468	π*(C5-C6)	0.27635	17.15	0.28	0.063
π(C7-C8)	1.66468	π*(C10-C11)	0.45451	24.81	0.25	0.073
σ(C8-C11)	1.97445	σ*(C10-C11)	0.03685	4.58	1.25	0.068
σ(C8-H17)	1.97753	σ*(C10-C11)	0.03685	4.57	1.05	0.062
π(C10-C11)	1.60721	π*(C3-C4)	0.26502	20.39	0.26	0.067
π(C10-C11)	1.60721	π*(C5-C6)	0.27635	18.10	0.30	0.068
π(C10-C11)	1.60721	π*(C7-C8)	0.29306	15.41	0.30	0.062
π(N13-O15)	1.98771	π*(N13-O15)	0.59980	6.75	0.35	0.051
LP (1) O1	1.96016	σ*(C2-C3)	0.07077	4.90	0.96	0.062
LP (1) O1	1.96016	σ*(C10-C11)	0.03685	6.54	1.06	0.074
LP (2) O1	1.73570	π*(C2-O9)	0.29388	37.46	0.31	0.097
LP (2) O1	1.73570	π*(C10-C11)	0.45451	29.18	0.33	0.092
LP (2) O9	1.81578	σ*(O1-C2)	0.13198	40.00	0.50	0.128
LP (2) O9	1.81578	σ*(C2-C3)	0.07077	18.33	0.68	0.102
LP (3) Cl12	1.91254	π*(C3-C4)	0.26502	14.58	0.31	0.063
LP (2) O14	1.89760	σ*(C3-N13)	0.09592	11.82	0.54	0.072
LP (2) O14	1.89760	σ*(N13-O15)	0.08819	18.03	0.60	0.094
LP (3) O14	1.38939	σ*(N13-O14)	0.07356	5.58	0.61	0.061
LP (3) O14	1.38939	π*(N13-O15)	0.59980	150.01	0.14	0.131
LP (2) O15	1.89348	σ*(C3-N13)	0.09592	11.77	0.54	0.071
LP (2) O15	1.89348	σ*(N13-O14)	0.07356	18.20	0.62	0.096

[a]Stabilization (delocalization) energy. [b]Energy difference between i (donor) and j (acceptor) NBO orbitals. [c]Fock matrix element i and j NBO orbitals

ACKNOWLEDGMENTS

The authors thank the PG and Research Department of Physics, N.M.S.S.V.N.College, Nagamalai, Madurai19, for providing the Gaussian 09 program package. The SAIF, IIT, Chennai shall be duly acknowledged for recording the FT-IR, FT-Raman and UV-Visible spectra.

CONFLICT OF INTEREST:

We declare no conflict of interest.

AUTHORS CONTRIBUTION

Surya S. Mohan: Writing- Original draft preparation, Theoretical calculations, Experimental characterizations.

M.R.Meera: Supervision, Writing- Reviewing and Editing, Result analysis

A. Rathika: Supervision, Writing- Reviewing and Editing.

R. Premkumar[4]: In vitro cytotoxicity analysis, Molecular docking, Result analysis

REFERENCES

1. Sechi M, Rizzi G, Bacchi A, Carcelli M, Rogolino D, Pala N, Sanchez TW, Taheri L, Dayam R, Neamati N, Designand synthesis of novel dihydroquinoline-3-carboxylic acidsas HIV-1 integrase inhibitors, Bioorganic & Medicinal Chemistry, 2009; 17(7):2925-2935. https://doi.org/10.1016/j.bmc.2008.10.088 PMid:19026554

2. Konakanchi R, Prabhakara Rao K, Reddy N, Prashanth J, Zinc (II) complex: Spectroscopic, physicochemical calculations, anti-inflammatory and in silico molecular docking studies, Journal of Molecular Structure, 2022; 1263:133070. https://doi.org/10.1016/j.molstruc.2022.133070

3. Konduri S, Pogaku V, Prashanth J, Siva Krishna V, Sriram D, Basavoju S, Behera JN, Prabhakara Rao K, Sacubitril-Based Urea and Thiourea Derivatives as Novel Inhibitors for Anti-Tubercular against Dormant Tuberculosis, Chemistry Select, 2021; 6:3869 - 3874. https://doi.org/10.1002/slct.202004724

4. Valarmathi T, Premkumar R, Meera MR, Milton Franklin Benial A, Spectroscopic, quantum chemical and molecular docking studies on 1-amino-5-chloroanthraquinone: A targeted drug therapy for thyroid cancer, Spectrochimica Acta Part A 2021; 255:119659. https://doi.org/10.1016/j.saa.2021.119659 PMid:33751957

5. Prashanth J, Kishan Ojha J, Venkatram Reddy B, Ramana Rao G, Experimental and theoretical study of 3-methyl-4-nitrobenzoic acid using DFT and IVP methods, Journal of Physics: Conference Series, 2016; 759:012057. https://doi.org/10.1088/1742-6596/759/1/012057

6. Konduri S, Prashanth J, Siva Krishna V, Sriram D, Behera JN, Siegel D, Prabhakara Rao K, Design and synthesis of purine connected piperazine derivatives as novel inhibitors of Mycobacterium tuberculosis, Bioorganic & Medicinal Chemistry Letters, 2020; 30:127512. https://doi.org/10.1016/j.bmcl.2020.127512 PMid:32871269

7. Prashanth J, Konakanchi R, Venkatram Reddy B, Barrier potentials, molecular structure, force filed calculations and quantum chemical studies of some bipyridine di-carboxylic acids using the experimental and theoretical using (DFT, IVP) approach, Molecular Simulation, 2019; 45:1353-1383. https://doi.org/10.1080/08927022.2019.1634807

8. Frisch MJ, Trucks GW, Schlegel HB et al, Gaussian 09, Revision C. 02, Gaussian Inc., Wallingford CT, 2009.

9. Jamroz MH, Vibrational Energy Distribution Analysis VEDA 4.0 Program, Warsaw, 2004.

10. Gauss View, Version 5, Ray Dennington, Todd Keith and John Milam, Semichem Inc., Shawnee MissionKS, 2009.

11. Pandimeena G, Premkumar R, Mathavan T, Milton Franklin Benial A, Spectroscopic, Quantum chemical and Molecular docking Studies on Methyl 6-aminopyridine-3-carboxylate: A potent bioactive agent for the treatment of sarcoidosis, Journal of Molecular Structure, 2021; 1231:129996. https://doi.org/10.1016/j.molstruc.2021.129996

12. Mohamed Asath R, Premkumar R, Mathavan T, Milton Franklin Benial A, Structural, spectroscopic and molecular docking studies on 2-amino-3-chloro-5-trifluoromethyl pyridine: A potential bioactive agent, Spectrochimica Acta Part A, 2017; 175:51-60. https://doi.org/10.1016/j.saa.2016.11.037 PMid:28012392

13. Suresh DM, Amalanathan M, Sebastian S, Sajan D, Hubert Joe I, Bena Jothy V, Nemec I, Vibrational spectral investigation and natural bond orbital analysis of pharmaceutical compound 7-Amino-2,4-dimethylquinolinium formate - DFT approach, Spectrochimica Acta Part A, 2013; 115:595-602. https://doi.org/10.1016/j.saa.2013.06.077 PMid:23872018

14. Varsanyi G, Assignments for Vibrational Spectra of Seven Hundred Benzene Derivatives, Vol. I, Adam Hilger, London, 1974.

15. Premkumar R, Shamima Hussain, Naidu Dhanpal Jayram, Stève-Jonathan Koyambo-Konzapa, Revathy MS, Mathavan T, Milton Franklin Benial A, Adsorption and Orientation Characteristics of 1-Methylpyrrole-2-carbonyl chloride using SERS and DFT Investigations, Journal of Molecular Structure, 2021; 1253:132201. https://doi.org/10.1016/j.molstruc.2021.132201

16. Glendening ED, Reed AE, Carpenter JE, Weinhold F, NBO Version 3.1, TCI, University of Wisconsin, Madison, 1998.

17. Demircioğlu Z, AlbayrakKaştaş C, Büyükgüngör O, Theoretical analysis (NBO, NPA, Mulliken Population Method) and molecular orbital studies (hardness, chemical potential, electrophilicity and Fukui function analysis) of (E)-2-((4-hydroxy-2-methylphenylimino)methyl)-3-methoxyphenol, Journal of Molecular Structure, 2015; 1091:183-195. https://doi.org/10.1016/j.molstruc.2015.02.076

18. Koyambo-Konzapa SJ, Premkumar R, Berthelot Saïd Duvalier RV, Gilbert Yvon MK, Nsangou M, Milton Franklin Benial A, Electronic, spectroscopic, molecular docking and molecular dynamics studies of neutral and zwitterionic forms of 3, 4-dihydroxy-L-phenylalanine: A novel lung cancer drug, Journal of Molecular Structure, 2022; 1260:132844. https://doi.org/10.1016/j.molstruc.2022.132844

19. Mohamed Asath R, Premkumar R, Mathavan T, Milton Franklin Benial A, Structural, spectroscopic and molecular docking studies on 2-amino-3-chloro-5-trifluoromethyl pyridine: A potential bioactive agent, Spectrochimica Acta Part A, 2017; 175: 51-60. https://doi.org/10.1016/j.saa.2016.11.037 PMid:28012392

20. Premkumar R, Hussain S, Koyambo-Konzapa SJ, et al, SERS and DFT investigations of methyl 4-bromo-1H- pyrrole-2-carboxylate adsorbed on silver and gold substrates: In perspective of biosensor applications, Journal of Molecular Structure, 2021; 1236: 130272. https://doi.org/10.1016/j.molstruc.2021.130272

21. Avdović EH, Milanović ZB, Živanović MN, Šeklić DS, Radojević ID, Čomić LR, Marković ZS, Synthesis, spectroscopic characterization, biological activity, DFT and molecular docking study of novel 4-hydroxycoumarine derivatives and corresponding palladium (II) complexes, Inorganica Chim Acta 2020; 504:119465. https://doi.org/10.1016/j.ica.2020.119465

22. Gunduz SK, Budama Kilinc Y, Bicak B, Gok B, Belmen B, Aydogan F, Yolacan C, New coumarin derivative with potential antioxidant activity: Synthesis, DNA binding and in silico studies (Docking, MD, ADMET), Arabian Journal of Chemistry 2023; 16(2):104440. https://doi.org/10.1016/j.arabjc.2022.104440

23. Dhawan S, Kerru N, Awolade P, Singh-Pillay A, Saha ST, Kaur M, Singh P, Synthesis, computational studies and antiproliferative activities of coumarin-tagged 1,3,4-oxadiazole conjugates against MDA-MB-231 and MCF-7 human breast cancer cells, Bioorganic Medicinal Chemistry, 2018; 26(21):5612-5623. https://doi.org/10.1016/j.bmc.2018.10.006 PMid:30360952

24. Wang Y, Ai J, Wang Y, Chen Y, Wang L, Liu G, Geng M, Zhang A, Synthesis and cMet Kinase Inhibition of 3,5-Disubstituted and 3,5,7-Trisubstituted 29 Quinolines: Identification of 3-(4-Acetylpiperazin-1-yl)-5-(3-nitrobenzylamino)-7-(trifluoromethyl) quinoline as a Novel Anticancer Agent, Journal of Medicinal Chemistry 2011; 54:2127- 2142. https://doi.org/10.1021/jm101340q PMid:21405128

25. Almutairi MS, Alanazi AM, Al-Abdullah ES, et al., FT-IR and FT-Raman spectroscopic signatures, vibrational assignments, NBO, NLO analysis and molecular docking study of 2-{[5-(adamantan-1-yl)-4-methyl-4H-1,2,4-triazol-3-yl]sulfanyl}-N,N-dimethylethanamine, Spectrochimica Acta Part A, 2015; 140:1-14. https://doi.org/10.1016/j.saa.2014.12.064 PMid:25579797